Estimation of ecosystem evapotranspiration in a *Robinia pseudoacacia* L. plantation with the use of the eddy covariance technique and modeling approaches

Nikos Markos and Kalliopi Radoglou

Nikos Markos
Kalliopi Radoglou (corresponding author)
Department of Forestry and Management of
    Environment and Natural Resources,
Democritus University of Thrace,
N. Orestiada,
Greece
E-mail: *kradoglo@fmenr.duth.gr*

ABSTRACT

The eddy covariance technique provides reliable ecosystem-level evapotranspiration (ET) measurements. These measurements, when combined with models and satellite products, could offer high spatiotemporal coverage and valuable mechanistic interpretation of the underlying processes. This study address one-year eddy covariance measurements from a *Robinia pseudoacacia* site in Northern Greece and remote sensing products: we (a) provide a medium-term description of daily ET fluxes for a *R. pseudoacacia* plantation in a degraded land, (b) assess the contribution of environmental drivers (e.g. net radiation, temperature etc.) on ET and (c) evaluate a simple satellite and meteorological driven model for larger-scale applications, based on the Land Surface Water Index (LSWI) and the FAO approach. *R. pseudoacacia* was found to have quite high water consumption, especially during leaf expansion. Net radiation and soil water content had the greatest effect on ecosystem evapotranspiration. LSWI was found to be correlated with both soil water content and evapotranspiration. Its use as an index for water limitation in models leads to high accuracy when compared to ET measurements. Our results (a) provide a significant contribution to the assessment of *R. pseudoacacia* ecophysiology and (b) highlight the potential of accurate ecosystem ET estimation with simple modeling approaches.

Key words │ black locust, deciduous forest, eddy covariance, evapotranspiration, Land Surface Water Index, restoration, *Robinia pseudoacacia*, transpiration

HIGHLIGHTS

- The eddy covariance method contributes to the better knowledge of the species ecophysiology, as well as its performance under highly degraded soils.
- An evapotranspiration model, evaluated against the eddy covariance measurements, appears to give a very good performance.
- Land Surface Water Index was found to correlate well with ecosystem evapotranspiration and can be used as a crop coefficient scalar.

INTRODUCTION

Evapotranspiration (ET) is one of the greatest components of energy fluxes and water cycling in the atmosphere (Katul *et al.* 2012). It is responsible for the returning of up to 2/3 of precipitation water back to the atmosphere on average globally (Jasechko *et al.* 2013; Wei *et al.* 2017; Yao *et al.* 2017), an amount that can be as high as 95% in dry ecosystems (Raz-Yaseef *et al.* 2010; Stoy *et al.* 2019). The accurate estimation of evapotranspiration is essential for a better understanding of the global water cycle (Cheng *et al.* 2011) and the improvement of water resource management (Mu *et al.* 2013a; Paschalis *et al.* 2018).

For ET estimation, several methods have been developed, including the use of the eddy covariance method (Baldocchi 2014), the Bowen Ratio (Scott *et al.* 2006), sap flow, large aperture scintillometers, lysimeters and others (Allen *et al.* 2011). The eddy covariance method is considered the most reliable and state-of-the-art technique for accurate ET measurement at the field scale (Zhang *et al.* 2014; Saitta *et al.* 2020).

All methods mentioned above can cover small to medium-sized areas. The estimation of ET for larger areas is performed with the use of ET models. Several ET modeling approaches exist with different degrees of complexity (Chen & Liu 2020). The basis of those models is solving the energy balance equation using the well-known Penman-Monteith equation (Allen *et al.* 1998). ET models can be summarized into two different categories: (a) those that are based on the land surface temperature (LST), which is closely linked to ecosystem water status and thus ET (Bastiaanssen *et al.* 1998; Anderson *et al.* 2007; Mu *et al.* 2013b; Chen & Liu 2020) and (b) those that are based on the crop coefficient approach, the so-called FAO approach (Allen *et al.* 1998). The actual evapotranspiration was estimated as the product of reference evapotranspiration (ET0) multiplied by a factor called crop coefficient (Kc).

Both approaches have significantly benefited from the advantages that remote sensing is offering for large scale monitoring. The first category of models uses the thermal bands of Modis or Landsat satellites to estimate LST by applying quite sophisticated approaches (Anderson *et al.* 2012; Mu *et al.* 2013b). However, as satellite thermal bands are provided in lower spatial resolutions when the modeling applications refer to smaller areas, there is a need for downscaling with special algorithms (Agam *et al.* 2007; Gao *et al.* 2012).

The second category has been so far following a more semi-empirical approach. While reference evapotranspiration is estimated as a function of environmental parameters, the crop coefficients are empirical species, specific factors, fluctuating during the year according to the species' growth stage (Allen *et al.* 1998; Pereira *et al.* 2021). In the past few years, satellite vegetation indices have been recognized to offer great advantages in crop coefficient modeling (Pereira *et al.* 2021). So far, several studies have used satellite spectral indices to represent the seasonal fluctuation of crop coefficients, such as NDVI (Hunsaker *et al.* 2005; Drerup *et al.* 2017; French *et al.* 2020), or relative indices, like EVI and Soil Adjusted Vegetation Index (SAVI) (Guerschman *et al.* 2009; Glenn *et al.* 2011; He *et al.* 2019). Most of the studies that follow similar approaches refer to agricultural sites, which means that water availability is not a marginal factor, so NDVI and EVI can represent the phenological status. However, it is difficult to describe the water stress effects. In satellite primary productivity models that use the light use efficiency approach (Monteith 1972), the Land Surface Water Index (LSWI), (Gao 1996)) was widely used as a representative of ecosystem water status (Xiao 2004; Mahadevan *et al.* 2008; Chen *et al.* 2011; Bao *et al.* 2016). The index is related to the total canopy water content (Gao 1996), and thus it could potentially represent both the canopy growth stage and water stress. This approach can provide further benefits; the vegetation indices mentioned can be acquired with a high spatial resolution, such as Sentinel 2, making the applications more suitable for small or medium-sized areas.

Modeling applications have been mainly focused on agricultural sites or natural ecosystems. On the other hand, the applications in forest plantations on disturbed or degraded land, like black locust plantations (Kanzler *et al.* 2020), are generally missing.

Black locust (*Robinia pseudoacacia* L.) is a medium-sized deciduous species. Although it is considered an

invasive species in Europe, it has already become a very common component of both economy and culture in many European countries (Vítková *et al.* 2017). Even though the use of the species in forest plantations has met a lot of criticism, the species has a long history of use in restoration projects due to its unique characteristics to adapt to marginal sites. It is a fast-growing, drought-tolerant and low demand species, able to grow in poor-nutrient areas (Nicolescu *et al.* 2020). Because of these unique characteristics, the species has become very common in reclamation projects for disturbed lands, such as former coal mines (Skousen & Zipper 2014; Carl *et al.* 2017; Vítková *et al.* 2017; Nicolescu *et al.* 2020). In Europe, black locust has been studied for a long time, with the studies being focused more on its economic value than ecology (Vítková *et al.* 2017). Over the last few years, many studies of the species have been mainly from the Loess Plateau in China (Wang *et al.* 2015; Jiao *et al.* 2018; Miyazawa *et al.* 2018; Zhao *et al.* 2018). Despite that, there are things about its ecology and ecophysiology that remain elusive.

The aim of this study is (a) to provide a medium-term presentation of measurements of daily ET fluxes for a tree plantation with the use of the eddy covariance method, (b) to assess the contribution of the main environmental driving parameters of the ET fluxes for the specific site and (c) to provide a simple, but accurate methodology for the extrapolation of the eddy tower measurements to greater scales with the use of a hybrid satellite and meteorological driven model, based on high spatial analysis vegetation indices from the Sentinel 2 satellite.

MATERIALS AND METHODS

Study site

The site is located on a flat field of about $5 \times 10^5 \, \text{m}^2$ (40.59 °N, 21.65 °E) that is part of a greater planted area of about $24 \times 10^6 \, \text{m}^2$ in the restored areas of the Western Macedonia Lignite Center, in Northern Greece (Figure 1). The dominant species of the plantations is *Robinia pseudoacacia*, a deciduous broadleaf species, which accounts for 95% of the total area of the plantations. The plantations consist of mature and younger trees, due to the continuous

restoration and plantation process of more than 20 years. The age of the trees at the study site is about 20 years. The mean tree height in the study site is 13.5 m and is relatively homogenous. *Robinia pseudoacacia* is a fast-growing species that can reach its maximum height before the age of 20 years (Nicolescu *et al.* 2020). The seasonal fluctuation of the Enhanced Vegetation Index (EVI) in the plantation, as estimated from the Sentinel 2 imagery, for a five-year period (2016–2020) is steady (see supplementary material). EVI is an index closely related to Leaf Area Index (LAI) (area of transpiration). Understory vegetation consists mainly of perennial grasses, with *Cynodon dactylon* being the dominant one. The growing period of the understory grass starts after leaf fall, as the leaves of black locust are very thin and delicate, resulting in a very quick decomposition, and it is active until the trees' leaf expansion at the beginning of May. The substrate consists of deposition material from the mining process that, in general, is very depleted and poor. It is characterized by alkaline pH and classified from moderately coarse to fine soils (Papadopoulos *et al.* 2015). Mean annual precipitation for the ten-year period in question (2010–2020) is $510 \pm 156 \, \text{mm}$, and mean annual temperature for the same period is $13.36 \pm 0.92 \, °\text{C}$, as estimated from the nearby meteorological station of the National Observatory of Athens (http://penteli.meteo.gr/stations/amyntaio/).

Meteorological and eddy covariance measurements

An eddy tower was installed at the end of July 2019, measuring continuously the exchanges of vapor, energy and CO_2 in the study area. The tower was installed in the middle of the study site in order to achieve a unidirectional footprint (no prevailing wind direction). The tower is equipped with an integrated IRGA analyzer and sonic anemometer (Irgason, Campbell Scientific Inc.) with an enhanced barometer (PTB 110, Vaisala Inc.), which perform CO_2/H_2O, three-component wind analysis and barometric pressure respectively and a full meteorological station, including, among others, a net radiometer (NR Lite2, Kipp and Zonen BV), a temperature/humidity probe (HygroClip2 Advanced, Rotronic Inc.) and three soil heat flux plates (HFP01, Hukseflux Thermal Sensors BV). The Irgason analyzer was placed in the top of the tower, at a total height of 17.5 m,
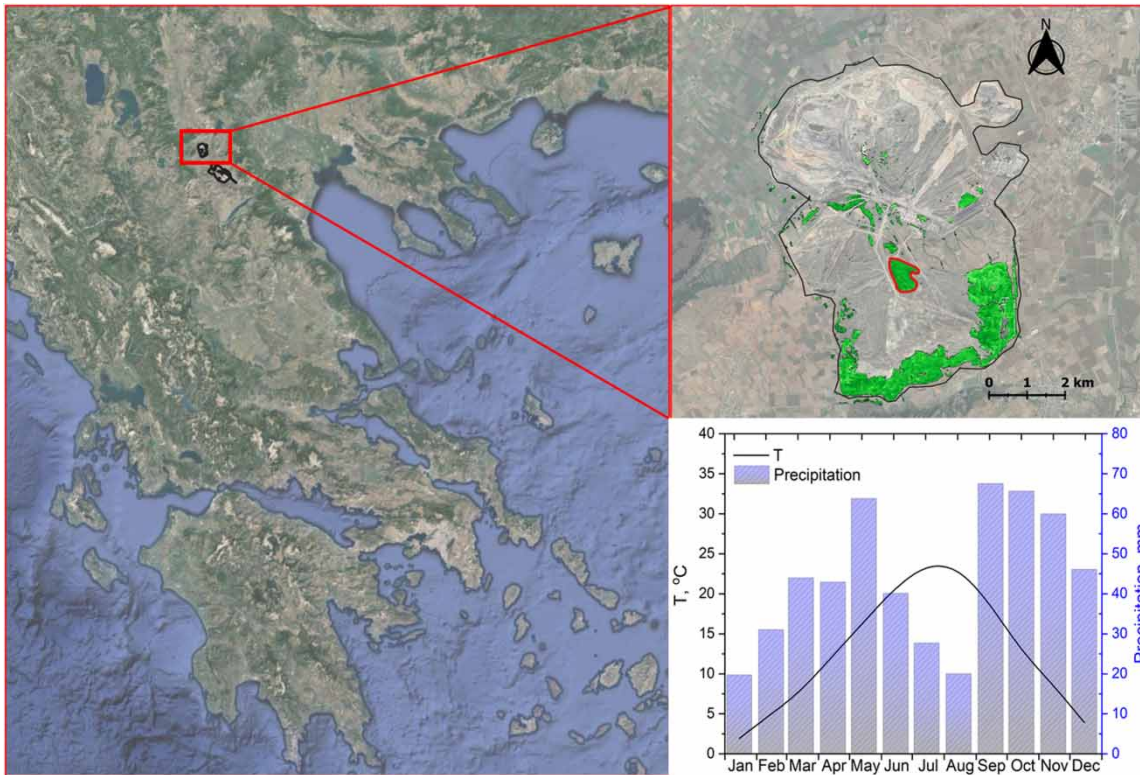
Figure 1 | Map and ombrothermic diagram for the study site. The eddy tower is installed inside the area marked with the red polygon (upper right). The ombrothermic diagram refers to the period 2010–2020. The full color version of this figure is available in the online version of this paper, at http://dx.doi.org/10.2166/ws.2021.142.

providing us an average fetch radius of 200 meters. Soil water content (SWC) is measured at 15 cm depth. Raw data are collected from a datalogger (CR1000X, Campbell Scientific Inc.) at a frequency of 10 Hz and processed on-site via an integrated analysis software (EasyFlux DL, Campbell Inc.) and post-processed with EddyPro 7 (Licor GmBh) with the use of the standardized eddy covariance methodology (Aubinet *et al.* 1999). The default time step of data acquisition was 30 min. Daily values were obtained by integrating or averaging the instantaneous values, depending on the parameter. Data gap-filling and flux partitioning were done using a standardized methodology (Reichstein *et al.* 2005). Data analysis covered the period from August 2019 to September 2020.

Reference evapotranspiration estimation

Reference evapotranspiration for the study site was calculated according to the FAO's methodology (Allen *et al.* 1998), Equation (1)

$$ET_0 = \frac{0.408(R_n - G) + \gamma \frac{900}{T + 273} u(es - ea)}{\Delta + \gamma(1 + 0.34u)} \tag{1}$$

where

ET_0 is the reference evapotranspiration (mm d^{-1})
R_n is the net radiation of the surface (MJ m^{-2} d^{-1})
G is the soil heat flux (MJ m^{-2} d^{-1})
γ is the psychrometric constant (kPa °C^{-1})
T is the mean daily air temperature (°C)
es is the saturated vapor pressure (kPa)
ea is the actual vapor pressure (kPa)
Δ is the slope vapor pressure curve (kPa °C^{-1})
u is the wind speed (m s^{-1}).

All the above parameters are estimated by the eddy tower on half-hourly time steps and then scaled to daily time steps. By definition, air temperature and wind speed

must be measured at the height of 2 meters or, if measured elsewhere, they have to be converted to that height. Our measurements were performed at the tower height (17.5 m) and no conversions were applied, to have a common reference with the other tower measurements.

Satellite image analysis

For the calculation of vegetation indices, we used the free-distributed products of Copernicus Sentinel 2 (https://sentinel.esa.int/web/sentinel/missions/sentinel-2), which offer the advantage of high resolution (10×10 m) and frequent acquisition. For our analyses, we used L2A products. The average acquisition of cloud-free images during the study period for our study site was four days.

Using five bands in total (blue, green, red, nir and swir), we estimated the time series of the vegetation indices Land Surface Water Index (LSWI), Normalized Difference Vegetation Index (NDVI), Enhanced Vegetation Index (EVI) and Normalized Difference Water Index (NDWI) (Table 1) for the whole study period.

All vegetation indices were estimated as the average ± standard deviation for the whole study site for cloud-free days, using the online analysis tool Sentinel-hub (https://www.sentinel-hub.com/). Sentinel 2 provides two SWIR bands, one at 1,565–1,655 nm and the other at 2,100–2,280 nm (https://sentinels.copernicus.eu). In this study, we used the SWIR1 (1,565–1,655 nm) band for the estimation of LSWI.

Table 1 | Definition and formulas for the vegetation indices used in the study

Index	Full name	Formula
NDVI	Normalized Difference Vegetation Index	$\dfrac{nir - red}{nir + red}$
EVI	Enhanced Vegetation Index	$2.5 * \dfrac{nir - red}{nir + 6.5 * red - 7.5 * blue + 1}$
LSWI	Land Surface Water Index	$\dfrac{nir - swir}{nir + swir}$
NDWI	Normalized Difference Water Index	$\dfrac{green - nir}{green + nir}$

Nir, red, green and swir stand for respective bands of Sentinel 2 imagery.

Modeling description and evaluation

For the modeling of ET, three different approaches were followed. The first one was the crop coefficient approach. Daily evapotranspiration was estimated as the product of reference evapotranspiration (as estimated from Equation (1)) multiplied by the crop coefficient Kc (Equation (2)). During this procedure, the daily values of Kc were estimated as the product of the maximum seasonal value (Kc_{max}) multiplied by the normalized fluctuation of the vegetation index (Equation (3)), according to Choudhury (1994).

$$ET = Kc * ET_0 = Kc_{max} * f(VI) * ET_0 \tag{2}$$

$$f(VI) = \frac{VI - VI_{min}}{VI_{max} - VI_{min}} \tag{3}$$

where

ET is the actual evapotranspiration (mm d^{-1})

ET_0 is the reference evapotranspiration (mm d^{-1}, Equation (1))

Kc is the crop coefficient (dimensionless)

VI, VI_{min} and VI_{max} are the running, minimum and maximum values of the corresponding spectral index during the study period.

Due to the specific conditions in the study site; that is, the two distinctive states of the vegetation (seasonally dominated either by grass or black locust canopy), we used two separate crop coefficients for different periods of the year. For the period between the leaf fall and new leaf expansion (November to April), during which the site's vegetation was dominated by the understory grass, the value of Kc_{max} equal to 1.2 was used (Allen *et al.* 2011). For the period after leaf expansion until leaf fall (May-October), during which the vegetation was dominated by the canopy, the value of Kc_{max} equal to 0.75 was used, which was the average maximum value of the ecosystem's Kc during the period of full leaf expansion, estimated as the ratio of ET/ET0 during the corresponding period, according to FAO methodology (Allen *et al.* 1998; Pereira *et al.* 2021). The value 0.75 for Kc_{max} used is inside the range of values for Kc of deciduous trees (0.45–1.2) proposed by FAO (Allen *et al.* 1998; Pereira *et al.* 2021). For the intermediate period from the beginning

of leaf expansion until full development (April-May), during which both understory vegetation and canopy are active, the average of the two values was used. The vegetation index used as a scalar for Kc$_{max}$ (Equation (3)) was better correlated to the measured ET fluxes (see results). As min and max values in Equation (3) minimum and maximum values of the indices during the study period were used and as the running values, the calculated indices, interpolated for the interval periods.

The second approach was similar to the one described above, with the difference that instead of ET0 we used the H$_2$O equivalent for net radiation (mm d^{-1}) as input to Equation (2). ET0 is a quantity that depends on many environmental parameters, as extensively described before. All the parameters do not have the same impact on actual ET. The subtraction of soil heat flux from net radiation should ideally be equal to the sum of latent and sensible heat flux (LE + H) which determines the total evaporative demand. We tried to further minimize the input parameters. An alternative version of the model was utilized. Total evaporative demand is not represented by reference evapotranspiration, but by the water equivalent of net radiation (mm d^{-1}). However, as the sum of LE + H are usually less than net radiation – global radiation (Rn-G) (Allen *et al.* 2011) and G is small compared to Rn, the water equivalent of Rn was multiplied by 0.88, a factor that resulted from the solving of the energy balance equation for our study site (see supplementary material).

The third approach was the derivation of an empirical formula from the regression of the measured daily evapotranspiration values with the satellite vegetation indices mentioned in the previous section (Table 1). Although this is the simplest approach, it lacks a mechanistic interpretation. While it can be useful for the specific site, it would be quite uncertain to use it in transferable applications.

For statistical analyses and diagram construction, the packages Origin 2020 and SPSS were used. The models' results were quantified against the measured ET values from the tower. The criteria used were the coefficients of determination from the linear regression analysis (R^2), the root mean square error (RMSE) (Equation (4)) and the Nash–Sutcliffe model coefficient (NSE) (Equation (5)), which determines the relative magnitude of the residual variance compared to the measured data variance (Nash &

Sutcliffe 1970).

$$RMSE = \sqrt{\frac{\sum_{i=1}^{N} (x_m^i - x_o^i)^2}{N}} \tag{4}$$

$$NSE = 1 - \frac{\sum_{i=1}^{N} (x_m^i - x_o^i)^2}{\sum_{i=1}^{N} (x_o^i - \overline{x_o})^2} \tag{5}$$

The assessment of the importance of relative contribution of each independent variable (net radiation (Rn), wind speed (WS), temperature (T) and vapor pressure deficit (VPD)) on ecosystem evapotranspiration was done by means of *P* values and standardized beta coefficients after the application of multiple regression analysis.

RESULTS AND DISCUSSION

Meteorological parameters

The seasonal fluctuation of meteorological data from the eddy tower is presented in Figure 2 and was used as inputs in Equation (1) to estimate reference evapotranspiration. The peak of net radiation (Rn) was observed during the period between mid-June to mid-July. Average Rn values were slightly higher during August 2020 compared to August 2019. Differences between 8/2019 and 8/2020 were observed at air temperature (T) and vapor pressure deficit (VPD) (Figure 2(b) and 2(c)). Both quantities were lower during 8/2020 compared to 8/2019 by about 2 °C and 0.3 kPa respectively. The precipitation and SWC are presented in Figure 2(d). The total precipitation amount for the whole study period (1/8/2019–27/9/2020) was 622 mm. Summer precipitation for 2020 (June – August) was quite high (170.8 mm), which accounted for 27.5% of total precipitation for the whole study period. SWC was kept high from the end of autumn until the middle of spring, when a rapid decrease was observed from the end of April until the end of May. In general, summer SWC values were quite high, as well as the precipitation. However, interannual differences were also observed, as the average % SWC during 8/2019 was 9.09 ± 1.55, while in
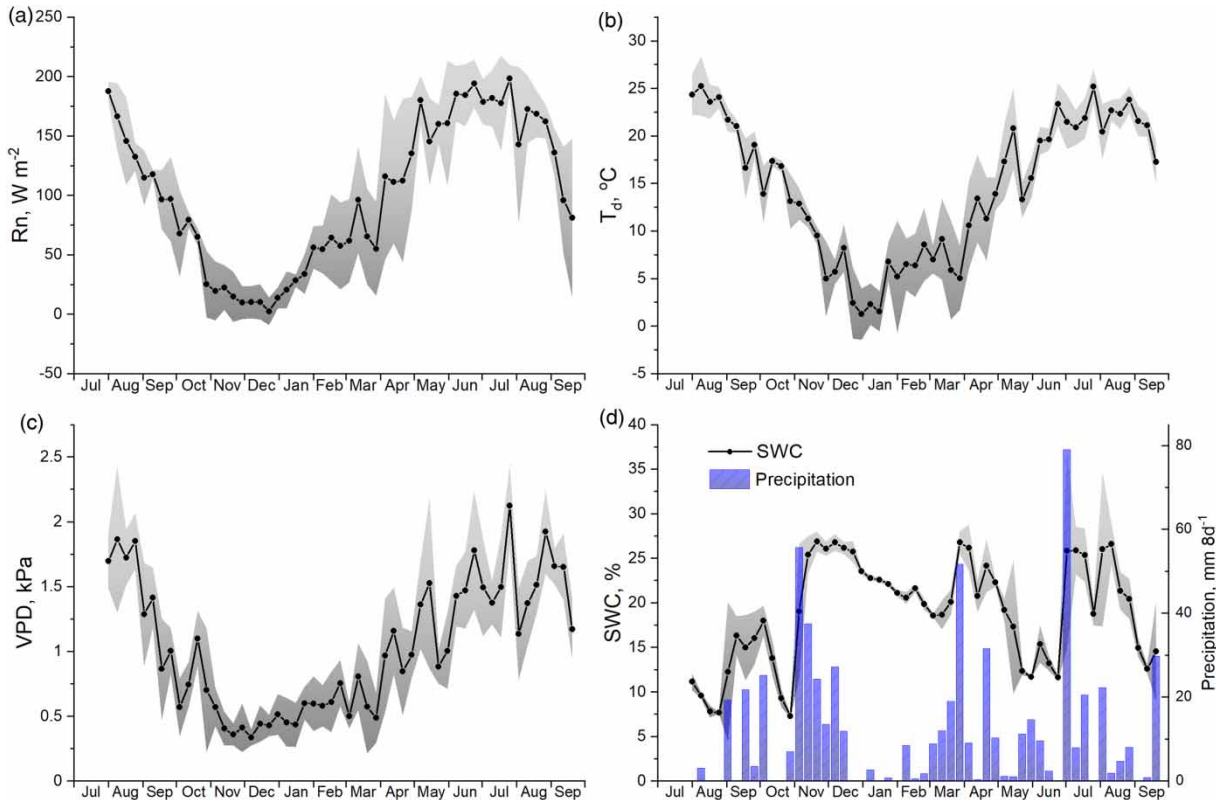
Figure 2 | Seasonal fluctuation of 8-day running averages of daily values of environmental parameters net radiation (a), air temperature (b), VPD (c) and SWC and precipitation (d) for the study period (2019–2020).

8/2020 23.54 ± 4.99 and the corresponding precipitation values were 3.1 and 36.9 mm, respectively. Finally, wind speed values did not appear to follow a clear seasonal pattern or have great differentiations, except for some higher values during the winter (data not shown).

Actual and reference evapotranspiration seasonal fluctuation

The seasonal fluctuation of both reference (ET0) as estimated by Equation (1) and actual evapotranspiration (ET), measured by the tower, is presented in Figure 3. The overall seasonal fluctuation of both quantities is generally following the annual pattern of net radiation and SWC (Figure 2). ET0 value is higher than the ET during the whole measured period. The lower annual rates are met during January, while two peaks can be found, one from May to the beginning of June and the other from July until the middle of August. Between those periods there is an intermediate
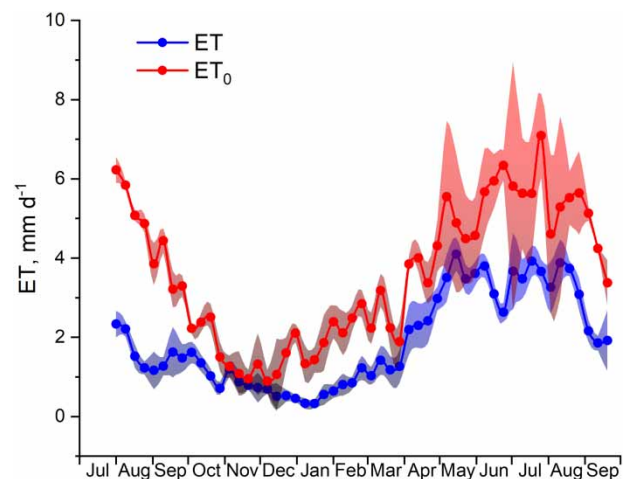

Figure 3 | Seasonal fluctuation of 8-day running averages of daily values of actual evapotranspiration (blue line) and reference evapotranspiration (red line) for the study period.

period of a sharp decline in the activity, which reflects the significant drop in rainfall and the decrease in SWC. The ET rates are considerably high from February to April,

before the leaf expansion, which can be attributed to the well-developed understory grass.

The period of the first peak (May-June) is similar to the period of ET maximization for the same species in the Loess Plateau in China (Miyazawa *et al.* 2018). The trees of the referred study were grown on an arid to semi-arid region with a different precipitation pattern and that's probably the reason for this very narrow peak. The peak during the beginning of May in our study site could be considered quite early, as during May the canopy was still under development and full leaf expansion is met about the middle of June (data not shown). It seems this species and the whole ecosystem, consequently, follow a strategy of very luxury water consumption during the canopy development. The result of this is rapid soil drying until the beginning of June, despite the considerable amount of precipitation during that period (Figure 2(d)). The excessive water consumption of black locust and the resulting decline in soil moisture has been reported in another study from a relative ecosystem in China (Liang *et al.* 2018). The estimated weighted annual sum of ET with eddy covariance for *Robinia pseudoacacia* is 595 mm, a value that is very close to the respective total sum of precipitation. Although this value is comparable to many deciduous broadleaf sites of the fluxnet network (fluxnet.org) (Fatichi & Pappas 2017), there are not many sites with the same species that are comparable, as was mentioned previously. In a relevant study, the average total ET of a two-year study for *R. pseudoacacia* was estimated to be about 208 mm y^{-1}. However, the average amount of precipitation was quite lower, about 262 mm y^{-1} (Jiao *et al.* 2018). Another study, (Fu *et al.* 2021) estimated the annual evapotranspiration for an *R. pseudoacacia* plantation under non-water stress conditions at 576.88 and 848.55 mm y^{-1} for a dry and a wet year respectively.

The assumptions mentioned before are made with a quite high degree of uncertainty, since our results refer to the total ecosystem fluxes and any partitioning of ecosystem ET to transpiration and soil evaporation was not applied. Although generally the contribution of transpiration to total ecosystem evapotranspiration in closed canopies is estimated to be up to 90% (Jasechko *et al.* 2013; Good *et al.* 2014; Li *et al.* 2019), in a relevant study in a *R. pseudoacacia* plantation, the corresponding proportion was estimated between 9.7 and 28.8% (Jiao *et al.* 2018), which can be considered quite low.

Spectral indices

Measured ET values are strongly correlated with all studied vegetation indices, with coefficients of determination ranging from 0.51 to 0.77. The strongest correlated index was the LSWI (R^2 = 0.77, Figure 4(a)). LSWI was used as the input parameter to describe the Kc scalar (Equation (3)) for the models based on reference evapotranspiration (Equation (2)). However, as the initial idea was to use a scalar for Kc that would be representative of both phenological and water status, the performance of LSWI versus ET was investigated under different water status scenarios. Given that daily ET seems to co-fluctuate seasonally with SWC (Figures 2 and 3), the effect of SWC to ET was assessed by comparing the respective values for the period of full leaf expansion (June – August, Figure 5(a)). This period limitation was followed to avoid the misinterpretation or noise that would come from data from the non-growing period. According to our findings, SWC is related to daily ET via an exponential function (Figure 5(a)) with a very high coefficient of determination (R^2 = 0.76, $P <$ 0.001). Based on this relationship, an apparent threshold of 15% SWC can be identified, below which ET values are strongly increasing with the increase of SWC and reach a plateau at about the value of 15% SWC. Following that threshold, the LSWI – ET values were separated into two sub-datasets, one that corresponded to SWC values greater than 15% and the other to SWC values less than 15% for the whole period of study, including the non-growing period. Regression analysis with the use of an exponential function was performed for the two datasets independently, as well as for the whole dataset together (Figure 5(b)). Based on the results of this analysis, ET is related to LSWI with exponential functions. Although ET values corresponding to SWC > 15% are significantly higher than the relative values that correspond to SWC < 15% for the same LSWI range, the use of a single exponential function applied to the whole dataset can be considered adequate to describe the ET dependence on LSWI for the whole SWC range, as nearly all values are inside the corresponding 95% prediction band (Figure 5(b)). Consequently, we can assume that LSWI is an appropriate index for the description of both the phenological stage and water status of our studied ecosystem. The accurate representation of water availability
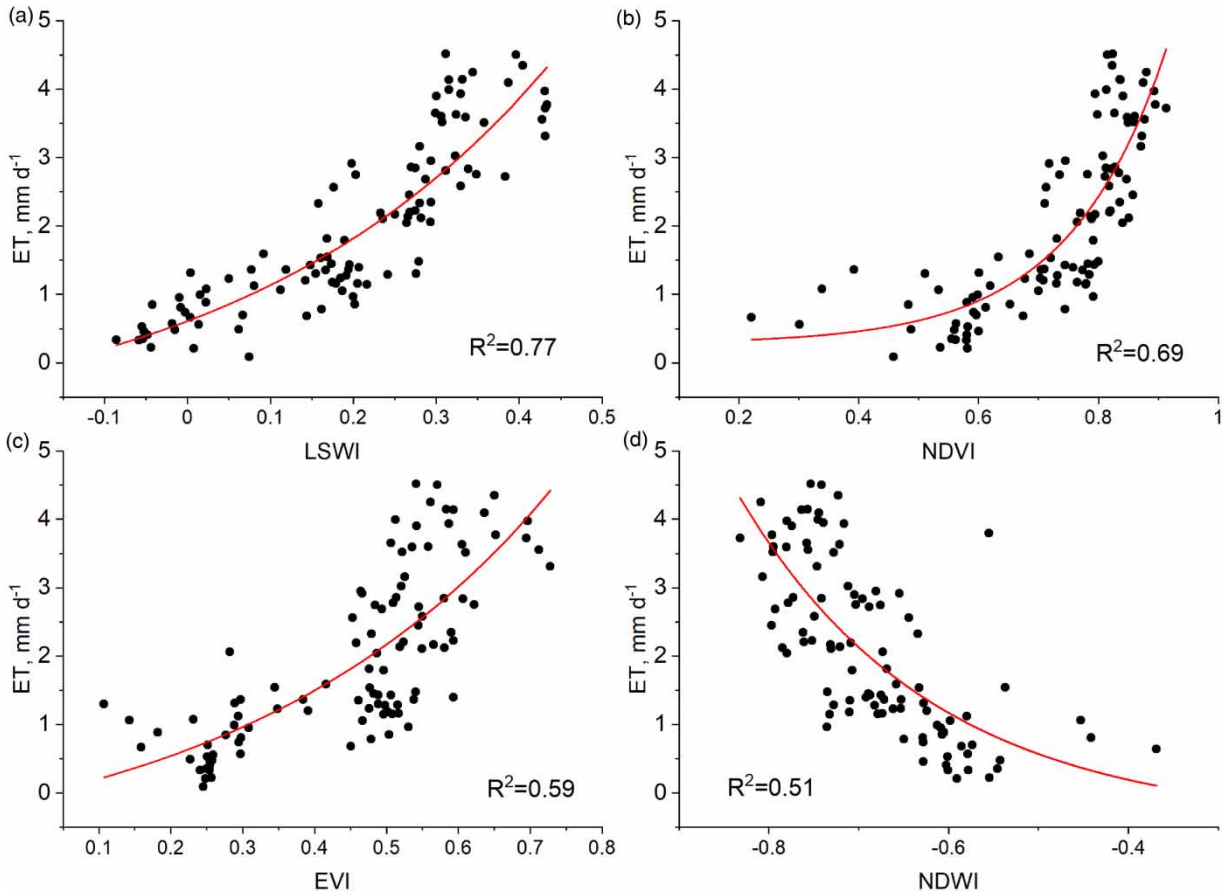
Figure 4 | Diagrams of correlation between daily ET values and and the coresponding satellite spectral indices LSWI (a), NDVI (b), EVI (c) and NDWI (d) for the study period.
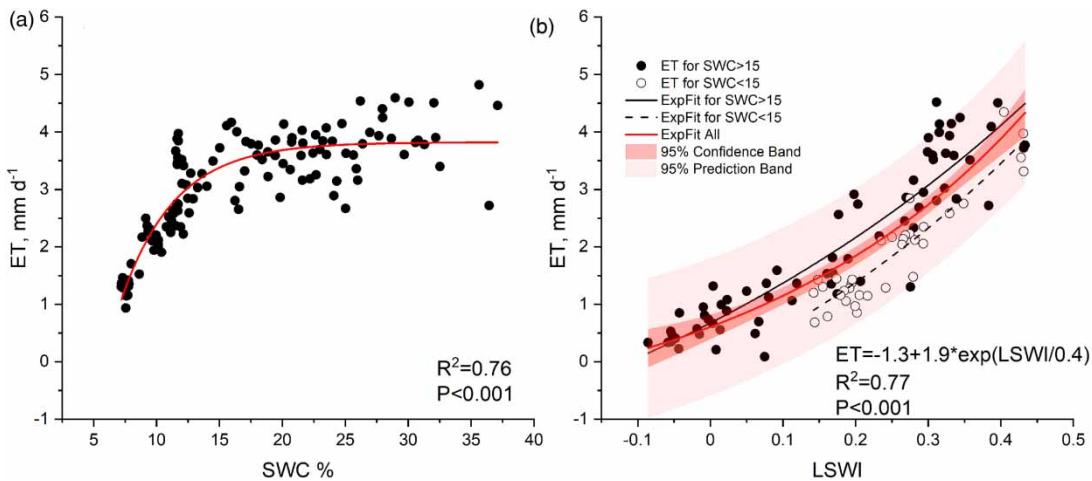

Figure 5 | Correlation of daily ET values with SWC during *Robinia*'s full leaf expansion (June – August, (a)) and correlation of daily ET values with LSWI for the whole study period (b). In (b), the closed circles stand for ET values that correspond to SWC > 15 and the open circles to SWC < 15. The solid black line is the regression of LSWI and ET for the first instance, the dashed black line for the second instance and the red line for the whole dataset. The 95% confidence and prediction bands refer to the regression for the whole dataset.

effects on ecosystems performance is one of the most important, yet demanding and uncertain procedures. Our findings highlight the great potential of LSWI to be used as a proxy for water limitations in our studied ecosystem and could act as a driver for further implications in other ecosystems.

Impact of environmental parameters on ET fluxes

Pearson R and regression coefficients R^2 between ET and ET0 daily values and the corresponding environmental parameters and LSWI are presented in Table 2. ET and ET0 are very strongly correlated with Rn, VPD, T and LSWI, while the correlation with wind speed is quite weaker for both quantities. The latter can be explained from the relative constant wind speed conditions throughout the study period. ET is better correlated with net radiation and LSWI, rather than ET0.

Both ET and ET0 are simultaneously affected by all the independent parameters mentioned above. The one-to-one comparison can lead to false conclusions about the real effect of each parameter on the final estimates. For example, net radiation (Rn) and temperature (T) follow similar seasonal fluctuation patterns, so their true relative impact cannot be distinguished in that way. Additional multiple regression analysis was applied, in order to estimate both the significance and the relative effect of each studied environmental parameter to ET and ET0. This was assessed by the P values and the standardized beta coefficients for each parameter. The results of the analysis are presented in Table 3.

According to the multiple regression analysis results, ET0 was significantly affected by all environmental parameters ($P < 0.001$), while the parameters that have greater effect on ET0 are net radiation and VPD, with beta values 0.64 and 0.39, respectively. The effect of temperature and wind speed are quite weaker. All independent parameters were positively correlated to ET0.

For actual ET, when LSWI was not included in the analysis, all environmental parameters were significant ($P < 0.001$) and Rn was the parameter with the strongest effect on ET. The second most important parameter was T. VPD was also found to have a significant effect; however, contrary to ET0 on this occasion, the effect is negative. The results of the analysis were altered when LSWI was included as an independent parameter in the analysis. In this case, both air temperature and VPD had no significant correlation to ET, as their P values are 0.27 and 0.71, respectively. The only important parameters are Rn, WS and LSWI. The parameter with the strongest effect was LSWI, followed by net radiation and wind speed.

Table 2 | Pearson R coefficients and regression coefficients between the measured environmental parameters and actual (ET) and reference evapotranspiration (ET0)

	ET		ET0	
	Pearson R	R^2	Pearson R	R^2
Rn	0.80	0.65	0.95	0.90
VPD	0.60	0.36	0.88	0.78
T	0.64	0.41	0.79	0.62
WS	−0.06	0.00	−0.03	0.00
LSWI	0.87	0.76	0.74	0.55
ET0	0.78	0.61	–	–

Net radiation (Rn), vapor pressure deficit (VPD), air temperature (T), wind speed (WS), Land Surface Water Index (LSWI).

Table 3 | Beta standardized coefficients and P values between actual (ET)/reference evapotranspiration (ET0) and the environmental parameters that are used as inputs to Equation (1)

	ET						ET0		
	LSWI excluded			LSWI included					
	Beta	Sig.	Tolerance	Beta	Sig.	Tolerance	Beta	Sig.	Tolerance
Rn	0.77	0.00	0.38	0.35	0.00	0.26	0.64	0.00	0.38
T	0.43	0.00	0.18	−0.06	0.27	0.14	0.05	0.00	0.18
VPD	−0.34	0.00	0.18	−0.02	0.71	0.16	0.39	0.00	0.18
WS	0.14	0.00	0.78	0.11	0.00	0.77	0.19	0.00	0.78
LSWI	–	–	–	0.68	0.00	0.29	–	–	–

Regarding Rn, these results are somehow expected, as Rn was the strongest component in the energy balance equation and thus determined the total evaporative demand. However, when T and VPD are analyzed, things are more complicated. Firstly, VPD is dependent on air temperature, so the use of both parameters in the same analysis can create some uncertainty. Secondly, while the increase of VPD increases the total evaporative demand, its effect on actual evapotranspiration could be either positive or negative (Massmann *et al.* 2019) as the increase of VPD leads to decrease in stomatal conductance (Dewar 2002).

According to the above, the model can be further simplified by using the water equivalent of net radiation (Rn) instead of reference evapotranspiration as a proxy for evaporative demand. This led to a model that relies on simplicity, without compromises in accuracy ($R^2 = 0.89$, RMSE = 0.53, NSE = 0.80). This can provide further advantages, as net radiation is a parameter that can be easily measured in the field or estimated from relevant satellite maps. The problem in this approach is the energy closure. The sum of LE + H does not equal Rn-G, with an uncertainty that can be as high as 30%, with usual values around 10–20% (Wilson *et al.* 2002; Allen *et al.* 2011; Burba 2013). In the case of our studied ecosystem, the relative value is estimated around 12% (see supplementary material).

Minimizing the input parameters, without making great compromises in accuracy, is of great importance in ecosystem modeling. According to our findings, not all environmental parameters have the same impact on ET fluxes for the studied ecosystem. Net radiation and LSWI can be adequate in order to provide an adequate estimation of ET on seasonal basis. Considering that net radiation is a quite easily measured or estimated parameter, that satellite imagery offers many advantages in its estimation (Hou *et al.* 2014; Verma *et al.* 2016; Chen *et al.* 2020). Its use along with LSWI could meet further applications in evapotranspiration modeling (Barr *et al.* 2012).

Model performance

The seasonal fluctuation of measured against modeled *ET* values, according to the three different modeling approaches, as well as the comparison of the measured and modeled values, is presented in Figure 6. The modeled values derived from Equation (2), using ET0 as a proxy for evaporative demand, are presented as Model 1, while the corresponding values that use the water equivalent of net radiation as a proxy for evaporative demand are presented as Model 2. Finally, the modeled ET values that come from the empirical regression of measured ET with LSWI, are presented as Model 3. All the three models show very good seasonal co-fluctuation and agreement with the measured values for their 8-day running averages (Figure 6(a)–6(c)), with comparable R^2 values, ranging from 0.85 to 0.89 (Figure 6(d)–6(f)). The same applies when RMSE and NSE are considered, with values ranging from 0.45–0.53 and 0.80–0.85, respectively. It must be mentioned that typically this comparison can be considered valid only for the cases of Model 1 and Model 2, because the regression analysis in the case of Model 3 comes from the same dataset with which the model was evaluated, so typically that can be considered as autocorrelation. However, our scope in this case is to present how the modeled values of the empirical function co-fluctuate seasonally with the measured values and what are the advantages or disadvantages compared to the more mechanistic models.

In general, ET models have been reported to perform quite satisfactory in several studies with R^2 coefficients ranging from 0.3 to 0.86 for crops (Battude *et al.* 2017; He *et al.* 2019; French *et al.* 2020) and 0.12–0.90 in natural forests (Nagler *et al.* 2005; Verstraeten *et al.* 2005; Cleugh *et al.* 2007; Velpuri *et al.* 2013; Yao *et al.* 2017). According to that, our modeling approach resulted in a model performance among the higher range.

However, the advantages of the developed model are not mainly concerned with its performance, but its simplicity. Although several models have used similar approaches; that is, to use satellite indices to model the crop coefficient, the most commonly used indices were NDVI and EVI (Hunsaker *et al.* 2005; Guerschman *et al.* 2009; Glenn *et al.* 2011; Drerup *et al.* 2017; He *et al.* 2019; French *et al.* 2020), which can adequately describe the phenological stage of the vegetation but are poorer for its water status. On the other hand, LSWI is related to the total vegetation water content, and as a result to both phenological stage and water status (Gao 1996). Additionally, LSWI has been found to have a strong correlation with LST (Mokhtari *et al.* 2019; Alexander 2020) and thus can be used as a substitute of thermal spectrum
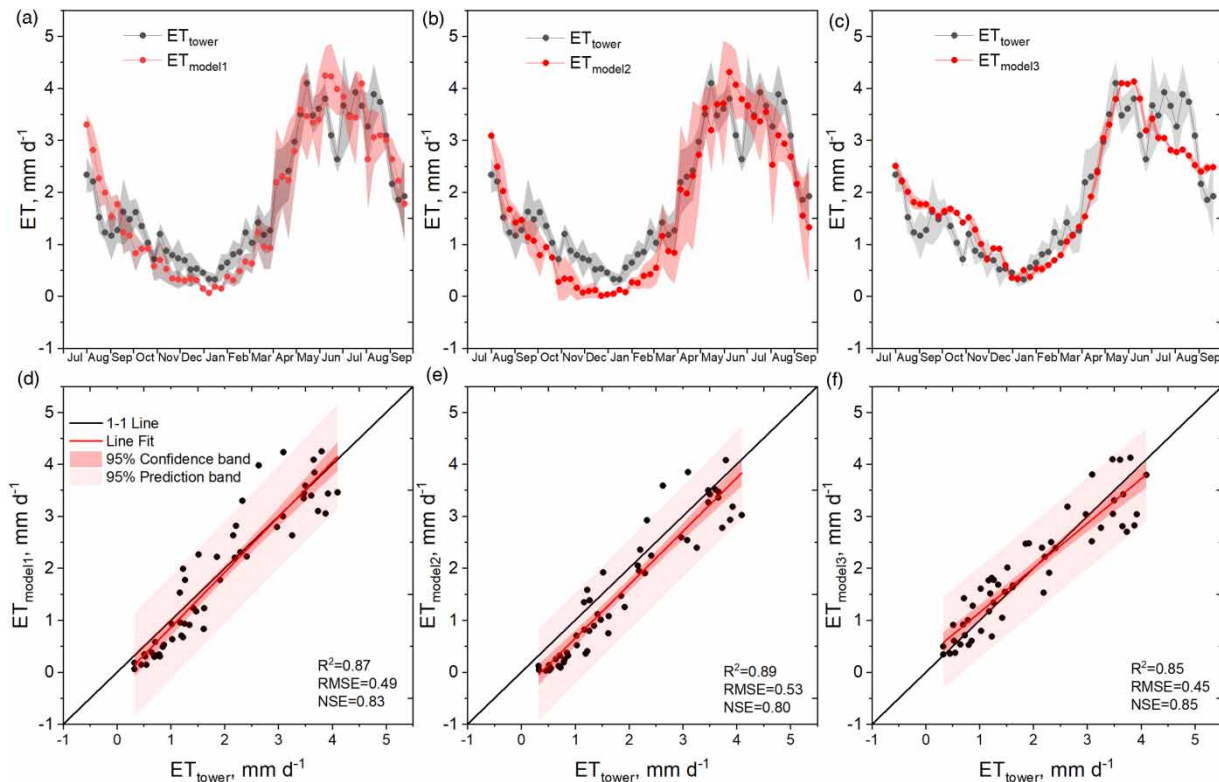
Figure 6 | Seasonal fluctuation of measured and modeled ET values at 8-day running averages; ET tower stands for the measured values from the eddy tower. ETmodel1 (a) and ETmodel2 stand for the modeled values using the reference evapotranspiration (b) and water equivalent of net radiation as proxy for evaporative demand. ETmodel3 stands for modeled ET values with the use of the empirical regression with LSWI. (c). The corresponding correlations of measured against modeled values with the three different modeling approaches (d)–(f), respectively. The coefficients of determination from the linear regression analysis (R2), the root mean square error (RMSE) and the Nash–Sutcliffe model efficiency coefficient (NSE).

(Sadeghi *et al.* 2015). Therefore, the use of LSWI, as a scalar to crop coefficient, could potentially work as a bridge between LST and crop coefficient based models. This is even more important if we considered that the studied ecosystem is not an agricultural site or a natural forest, but a plantation grown on a degraded site.

CONCLUSIONS

In this study we presented the results of more than one-year measurements and modeling of ecosystem evapotranspiration for a *Robinia pseudoacacia* plantation grown after restoration of highly disturbed land.

Reference evapotranspiration estimated from Equation (1) (ET0) has given a higher value from actually measured evapotranspiration (ET) from an eddy tower during the whole study period. A high value of ET was recorded in May to middle August. SWC is related to daily ET via an exponential function. The relationship between satellite spectral indices and the corresponding daily evapotranspiration values showed that LSWI was the most higher correlated index. From the environmental parameters, LSWI and Rn were those which had strong effect on ET. ET is dependent on LSWI and it is an appropriate index for the description of both phenological stage and water status of the studied ecosystem.

The results of this study contribute to the better understanding of the behavior *of Robinia pseudoacacia*, as well as the ecosystem processes of forest plantations grown on disturbed sites, and potentially they can lead to further investigation of the potential of minimization of the input parameters on ET models, without great compromises on model performance and accuracy.

In general, although *R. pseudoacacia* is already a species with an extensive distribution in Europe and worldwide, there are still many things to be studied concerning its ecology and behavior, and its contribution to the global carbon and water cycle. We believe that our findings can have a significant contribution in this direction.

ACKNOWLEDGEMENTS

FUNDING

DATA AVAILABILITY STATEMENT

Data cannot be made publicly available; readers should contact the corresponding author for details.

REFERENCES

Agam, N., Kustas, W. P., Anderson, M. C., Li, F. & Neale, C. M. U. 2007 A vegetation index based technique for spatial sharpening of thermal imagery. *Remote Sensing of Environment* **107**, 545–558.

Alexander, C. 2020 Normalised difference spectral indices and urban land cover as indicators of land surface temperature (LST). *International Journal of Applied Earth Observation and Geoinformation* **86**, 102013.

Allen, R. G., Pereira, L. S., Raes, D. & Smith M, W. A. B. 1998 Crop evapotranspiration – Guidelines for computing crop water requirements – FAO Irrigation and Drainage Paper 56, 300pp.

Allen, R. G., Pereira, L. S., Howell, T. A. & Jensen, M. E. 2011 Evapotranspiration information reporting: I. Factors governing measurement accuracy. *Agricultural Water Management* **98**, 899–920.

Anderson, M. C., Norman, J. M., Mecikalski, J. R., Otkin, J. A. & Kustas, W. P. 2007 A climatological study of evapotranspiration and moisture stress across the continental United States based on thermal remote sensing: 1. Model formulation. *Journal of Geophysical Research Atmospheres* **112**, 1–17.

Anderson, M. C., Allen, R. G., Morse, A. & Kustas, W. P. 2012 Use of Landsat thermal imagery in monitoring evapotranspiration and managing water resources. *Remote Sensing of Environment* **122**, 50–65.

Aubinet, M., Grelle, A., Ibrom, A., Rannik, Ü., Moncrieff, J., Foken, T., Kowalski, A. S., Martin, P. H., Berbigier, P., Bernhofer, C., Clement, R., Elbers, J., Granier, A., Grünwald, T., Morgenstern, K., Pilegaard, K., Rebmann, C., Snijders, W., Valentini, R. & Vesala, T. 1999 Estimates of the annual net carbon and water exchange of forests: the EUROFLUX methodology. *Advances in Ecological Research* **30**, 113–175.

Baldocchi, D. 2014 Measuring fluxes of trace gases and energy between ecosystems and the atmosphere – the state and future of the eddy covariance method. *Global Change Biology* **20**, 3600–3609.

Bao, G., Bao, Y., Qin, Z., Xin, X., Bao Yulong Bayarsaikan, S., Zhou, Y. & Chuntai, B. 2016 Modeling net primary productivity of terrestrial ecosystems in the semi-arid climate of the Mongolian Plateau using LSWI-based CASA ecosystem model. *International Journal of Applied Earth Observation and Geoinformation* **46**, 84–93.

Barr, A. G., van der Kamp, G., Black, T. A., McCaughey, J. H. & Nesic, Z. 2012 Energy balance closure at the BERMS flux towers in relation to the water balance of the White Gull Creek watershed 1999–2009. *Agricultural and Forest Meteorology* **153**, 3–13. https://doi.org/10.1016/j.agrformet.2011.05.017.

Bastiaanssen, W. G. M., Menenti, M., Feddes, R. A. & Holtslag, A. A. M. 1998 A remote sensing surface energy balance algorithm for land (SEBAL): 1. Formulation. *Journal of Hydrology* **212–213**, 198–212.

Battude, M., Al Bitar, A., Brut, A., Tallec, T., Huc, M., Cros, J., Weber, J. J., Lhuissier, L., Simonneaux, V. & Demarez, V. 2017 Modeling water needs and total irrigation depths of maize crop in the south west of France using high spatial and temporal resolution satellite imagery. *Agricultural Water Management* **189**, 123–136.

Burba, G. 2013 *Eddy Covariance Method for Scientific, Industrial, Agricultural and Regulatory Applications: A Field Book on Measuring Ecosystem Gas Exchange and Areal Emission Rates.* LI-COR Biosciences, Lincoln, USA.

Carl, C., Landgraf, D., van der Maaten-Theunissen, M., Biber, P. & Pretzsch, H. 2017 *Robinia pseudoacacia* L. Flower analyzed by using Unmanned Aerial Vehicle (UAV). *Remote Sensing* **9**, 1–19.

Chen, J. M. & Liu, J. 2020 Evolution of evapotranspiration models using thermal and shortwave remote sensing data. *Remote Sensing of Environment* **237**, 111594.

Chen, M., Zhuang, Q., Cook, D. R., Coulter, R., Pekour, M., Scott, R. L., Munger, J. W. & Bible, K. 2011 Quantification of terrestrial ecosystem carbon dynamics in the conterminous United States combining a process-based biogeochemical model and MODIS and AmeriFlux data. *Biogeosciences* **8**, 2665–2688.

Chen, J., He, T., Jiang, B. & Liang, S. 2020 Estimation of all-sky all-wave daily net radiation at high latitudes from MODIS data. *Remote Sensing of Environment* **245**, 111842.

Cheng, L., Xu, Z., Wang, D. & Cai, X. 2011 Assessing interannual variability of evapotranspiration at the catchment scale using satellite-based evapotranspiration data sets. *Water Resources Research* **47** (9), 1–11.

Choudhury, B. J. 1994 Synergism of multispectral satellite observations for estimating regional land surface evaporation. *Remote Sensing of Environment* **49**, 264–274.

Cleugh, H. A., Leuning, R., Mu, Q. & Running, S. W. 2007 Regional evaporation estimates from flux tower and MODIS satellite data. *Remote Sensing of Environment* **106**, 285–304.

Dewar, R. C. 2002 The Ball-Berry-Leuning and Tardieu-Davies stomatal models: synthesis and extension within a spatially aggregated picture of guard cell function. *Plant, Cell and Environment* **25**, 1383–1398.

Drerup, P., Brueck, H. & Scherer, H. W. 2017 Evapotranspiration of winter wheat estimated with the FAO 56 approach and NDVI measurements in a temperate humid climate of NW Europe. *Agricultural Water Management* **192**, 180–188.

Fatichi, S. & Pappas, C. 2017 Constrained variability of modeled T: ET ratio across biomes. *Geophysical Research Letters* **44** (13), 6795–6803. https://doi.org/10.1002/2017GL074041.

French, A. N., Hunsaker, D. J., Sanchez, C. A., Saber, M., Gonzalez, J. R. & Anderson, R. 2020 Satellite-based NDVI crop coefficients and evapotranspiration with eddy covariance validation for multiple durum wheat fields in the US Southwest. *Agricultural Water Management* **239**, 106266.

Fu, C., Song, X., Li, L. & Li, H. 2021 Study on vegetation water requirements of *Robinia pseudoacacia* and its mixed plantation in Loess Gully Region. *IOP Conference Series: Earth and Environmental Science* **643**, 012122.

Gao, B. C. 1996 NDWI – A normalized difference water index for remote sensing of vegetation liquid water from space. *Remote Sensing of Environment* **58**, 257–266.

Gao, F., Kustas, W. P. & Anderson, M. C. 2012 A data mining approach for sharpening thermal satellite imagery over land. *Remote Sensing* **4**, 3287–3319.

Glenn, E. P., Neale, C. M. U., Hunsaker, D. J. & Nagler, P. L. 2011 Vegetation index-based crop coefficients to estimate evapotranspiration by remote sensing in agricultural and natural ecosystems. *Hydrological Processes* **25**, 4050–4062.

Good, S. P., Soderberg, K., Guan, K., King, E. G., Scanlon, T. M. & Caylor, K. K. 2014 δ2 h isotopic flux partitioning of evapotranspiration over a grass field following a water pulse and subsequent dry down. *Water Resources Research* **50**, 1410–1432.

Guerschman, J. P., Van Dijk, A. I. J. M., Mattersdorf, G., Beringer, J., Hutley, L. B., Leuning, R., Pipunic, R. C. & Sherman, B. S. 2009 Scaling of potential evapotranspiration with MODIS data reproduces flux observations and catchment water balance observations across Australia. *Journal of Hydrology* **369**, 107–119.

He, M., Kimball, J. S., Yi, Y., Running, S. W., Guan, K., Moreno, A., Wu, X. & Maneta, M. 2019 Satellite data-driven modeling of field scale evapotranspiration in croplands using the MOD16 algorithm framework. *Remote Sensing of Environment* **230**, 111201.

Hou, J., Jia, G., Zhao, T., Wang, H. & Tang, B. 2014 Satellite-based estimation of daily average net radiation under clear-sky conditions. *Advances in Atmospheric Sciences* **31**, 705–720.

Hunsaker, D. J., Pinter, P. J. & Kimball, B. A. 2005 Wheat basal crop coefficients determined by normalized difference vegetation index. *Irrigation Science* **24**, 1–14.

Jasechko, S., Sharp, Z. D., Gibson, J. J., Birks, S. J., Yi, Y. & Fawcett, P. J. 2013 Terrestrial water fluxes dominated by transpiration. *Nature* **496**, 347–350.

Jiao, L., Lu, N., Fu, B., Wang, J., Li, Z., Fang, W., Liu, J., Wang, C. & Zhang, L. 2018 Evapotranspiration partitioning and its implications for plant water use strategy: evidence from a black locust plantation in the semi-arid Loess Plateau, China. *Forest Ecology and Management* **424**, 428–438.

Kanzler, M., Böhm, C. & Freese, D. 2020 The development of soil organic carbon under young black locust (*Robinia pseudoacacia* L.) trees at a post-mining landscape in eastern Germany. *New Forests* **52**, 47–68.

Katul, G. G., Oren, R., Manzoni, S., Higgins, C. & Parlange, M. B. 2012 Evapotranspiration: a process driving mass transport and energy exchange in the soil-plant-atmosphere-climate system. *Reviews of Geophysics* **50** (3), RG3002.

Li, X., Gentine, P., Lin, C., Zhou, S., Sun, Z., Zheng, Y., Liu, J. & Zheng, C. 2019 A simple and objective method to partition evapotranspiration into transpiration and evaporation at eddy-covariance sites. *Agricultural and Forest Meteorology* **265**, 171–182.

Liang, H., Xue, Y., Li, Z., Wang, S., Wu, X., Gao, G., Liu, G. & Fu, B. 2018 Soil moisture decline following the plantation of *Robinia pseudoacacia* forests: evidence from the loess plateau. *Forest Ecology and Management* **412**, 62–69.

Mahadevan, P., Wofsy, S. C., Matross, D. M., Xiao, X., Dunn, A. L., Lin, J. C., Gerbig, C., Munger, J. W., Chow, V. Y. & Gottlieb, E. W. 2008 A satellite-based biosphere parameterization for net ecosystem CO_2 exchange: Vegetation Photosynthesis and Respiration Model (VPRM). *Global Biogeochemical Cycles* **22** (2), GB2005.

Massmann, A., Gentine, P. & Lin, C. 2019 When does vapor pressure deficit drive or reduce evapotranspiration? *Journal of Advances in Modeling Earth Systems* **11**, 3305–3320.

Miyazawa, Y., Du, S., Taniguchi, T., Yamanaka, N. & Kumagai, T. 2018 Gas exchange by the mesic-origin, arid land plantation

species *Robinia pseudoacacia* under annual summer reduction in plant hydraulic conductance. *Tree Physiology* **38**, 1166–1179.

Mokhtari, A., Noory, H., Pourshakouri, F., Haghighatmehr, P., Afrasiabian, Y., Razavi, M., Fereydooni, F. & Sadeghi Naeni, A. 2019 Calculating potential evapotranspiration and single crop coefficient based on energy balance equation using Landsat 8 and Sentinel-2. *ISPRS Journal of Photogrammetry and Remote Sensing* **154**, 231–245.

Monteith, J. 1972 Solar radiation and productivity in tropical ecosystems. *Journal of Applied Ecology* **9**, 747–766.

Mu, Q., Zhao, M., Kimball, J. S., McDowell, N. G. & Running, S. W. 2013a A remotely sensed global terrestrial drought severity index. *Bulletin of the American Meteorological Society* **94**, 83–98.

Mu, Q., Zhao, M. & Running, S. W. 2013b MODIS global Terrestrial Evapotranspiration (ET) Product (NASA MOD16A2/A3) Collection 5. Algorithm Theoritical Basis Document. Available at: https://modis-land.gsfc.nasa.gov/pdf/MOD16ATBD.pdf.

Nagler, P. L., Scott, R. L., Westenburg, C., Cleverly, J. R., Glenn, E. P. & Huete, A. R. 2005 Evapotranspiration on western U.S. rivers estimated using the Enhanced Vegetation Index from MODIS and data from eddy covariance and Bowen ratio flux towers. *Remote Sensing of Environment* **97**, 337–351.

Nash, J. E. & Sutcliffe, J. V. 1970 River flow forecasting through conceptual models part I - a discussion of principles. *Journal of Hydrology* **10** (3), 282–290.

Nicolescu, V. N., Rédei, K., Mason, W. L., Vor, T., Pöetzelsberger, E., Bastien, J. C., Brus, R., BenčaÅ¥, T., Đodan, M., Cvjetkovic, B., Andrašev, S., La Porta, N., Lavnyy, V., Mandžukovski, D., Petkova, K., Roženbergar, D., Wąsik, R., Mohren, G. M. J., Monteverdi, M. C., Musch, B., Klisz, M., Perić, S., Keça, L., Bartlett, D., Hernea, C. & Pástor, M. 2020 Ecology, growth and management of black locust (*Robinia pseudoacacia* L.), a non-native species integrated into European forests. *Journal of Forestry Research* **31**, 1081–1101.

Papadopoulos, C., Gekaa, C., Pavloudakis, F., Roumpos, C. & Andreadou, S. 2015 Evaluation of the soil quality on the reclaimed lignite mine land in West Macedonia, Greece. *Procedia Earth and Planetary Science* **15**, 928–932.

Paschalis, A., Fatichi, S., Pappas, C. & Or, D. 2018 Covariation of vegetation and climate constrains present and future T/ET variability. *Environmental Research Letters* **13** (10), 0–18. https://doi.org/10.1088/1748-9326/aae267.

Pereira, L. S., Paredes, P., Hunsaker, D. J., López-Urrea, R. & Mohammadi Shad, Z. 2021 Standard single and basal crop coefficients for field crops. Updates and advances to the FAO56 crop water requirements method. *Agricultural Water Management* **243**, 106466.

Raz-Yaseef, N., Rotenberg, E. & Yakir, D. 2010 Effects of spatial variations in soil evaporation caused by tree shading on water flux partitioning in a semi-arid pine forest. *Agricultural and Forest Meteorology* **150**, 454–462.

Reichstein, M., Falge, E., Baldocchi, D. D., Papale, D., Aubinet, M., Berbigier, P., Bernhofer, C., Buchmann, N., Gilmanov, T., Granier, A. A., Grunwald, T., Havrankova, K., Ilvesniemi, H., Janous, D., Knohl, A., Laurila, T., Lohila, A., Loustau, D., Matteucci, G., Meyers, T., Miglietta, F., Ourcival, J.-M. M., Pumpanen, J., Rambal, S., Rotenberg, E., Sanz, M., Tenhunen, J., Seufert, G. G., Vaccari, F., Vesala, T., Yakir, D., Valentini, R., Grünwald, T., Havránková, K., Ilvesniemi, H., Janous, D., Knohl, A., Laurila, T., Lohila, A., Loustau, D., Matteucci, G., Meyers, T., Miglietta, F., Ourcival, J.-M. M., Pumpanen, J., Rambal, S., Rotenberg, E., Sanz, M., Tenhunen, J., Seufert, G. G., Vaccari, F., Vesala, T., Yakir, D. & Valentini, R. 2005 On the separation of net ecosystem exchange into assimilation and ecosystem respiration: review and improved algorithm. *Global Change Biology* **11**, 1424–1439.

Sadeghi, M., Jones, S. B. & Philpot, W. D. 2015 A linear physically-based model for remote sensing of soil moisture using short wave infrared bands. *Remote Sensing of Environment* **164**, 66–76.

Saitta, D., Vanella, D., Ramírez-Cuesta, J. M., Longo-Minnolo, G., Ferlito, F. & Consoli, S. 2020 Comparison of orange orchard evapotranspiration by eddy covariance, sap flow, and FAO-56 methods under different irrigation strategies. *Journal of Irrigation and Drainage Engineering* **146**, 05020002.

Scott, R. L., Huxman, T. E., Cable, W. L. & Emmerich, W. E. 2006 Partitioning of evapotranspiration and its relation to carbon dioxide exchange in a Chihuahuan Desert shrubland. *Hydrological Processes* **20**, 3227–3243.

Skousen, J. & Zipper, C. E. 2014 Post-mining policies and practices in the Eastern USA coal region. *International Journal of Coal Science and Technology* **1**, 135–151.

Stoy, P. C., El-Madany, T. S., Fisher, J. B., Gentine, P., Gerken, T., Good, S. P., Klosterhalfen, A., Liu, S., Miralles, D. G., Perez-Priego, O., Rigden, A. J., Skaggs, T. H., Wohlfahrt, G., Anderson, R. G., Coenders-Gerrits, A. M. J., Jung, M., Maes, W. H., Mammarella, I., Mauder, M., Migliavacca, M., Nelson, J. A., Poyatos, R., Reichstein, M., Scott, R. L. & Wolf, S. 2019 Reviews and syntheses: turning the challenges of partitioning ecosystem evaporation and transpiration into opportunities. *Biogeosciences* **16**, 3747–3775.

Velpuri, N. M., Senay, G. B., Singh, R. K., Bohms, S. & Verdin, J. P. 2013 A comprehensive evaluation of two MODIS evapotranspiration products over the conterminous United States: using point and gridded FLUXNET and water balance ET. *Remote Sensing of Environment* **139**, 35–49.

Verma, M., Fisher, J. B., Mallick, K., Ryu, Y., Kobayashi, H., Guillaume, A., Moore, G., Ramakrishnan, L., Hendrix, V., Wolf, S., Sikka, M., Kiely, G., Wohlfahrt, G., Gielen, B., Roupsard, O., Toscano, P., Arain, A. & Cescatti, A. 2016 Global surface net-radiation at 5 km from MODIS Terra. *Remote Sensing* **8** (9), 739.

Verstraeten, W. W., Veroustraete, F. & Feyen, J. 2005 Estimating evapotranspiration of European forests from NOAA-imagery

at satellite overpass time: towards an operational processing chain for integrated optical and thermal sensor data products. *Remote Sensing of Environment* **96**, 256–276.

Vítková, M., Müllerová, J., Sádlo, J., Pergl, J. & Pyšek, P. 2017 Black locust (*Robinia pseudoacacia*) beloved and despised: a story of an invasive tree in Central Europe. *Forest Ecology and Management* **384**, 287–302.

Wang, J. J., Hu, C. X., Bai, J. & Gong, C. M. 2015 Carbon sequestration of mature black locust stands on the Loess Plateau, China. *Plant, Soil and Environment* **61**, 116–121.

Wei, Z., Yoshimura, K., Wang, L., Miralles, D. G., Jasechko, S. & Lee, X. 2017 Revisiting the contribution of transpiration to global terrestrial evapotranspiration. *Geophysical Research Letters* **44**, 2792–2801.

Wilson, K., Goldstein, A., Falge, E., Aubinet, M., Baldocchi, D., Berbigier, P., Bernhofer, C., Ceulemans, R., Dolman, H., Field, C., Grelle, A., Ibrom, A., Law, B. E., Kowalski, A., Meyers, T., Moncrieff, J., Monson, R., Oechel, W., Tenhunen, J., Valentini, R. & Verma, S. 2002 Energy balance closure at FLUXNET sites. *Agricultural and Forest Meteorology* **113**, 223–243.

Xiao, X. 2004 Modeling gross primary production of temperate deciduous broadleaf forest using satellite images and climate data. *Remote Sensing of Environment* **91**, 256–270.

Yao, Y., Liang, S., Li, X., Chen, J., Liu, S., Jia, K., Zhang, X., Xiao, Z., Fisher, J. B., Mu, Q., Pan, M., Liu, M., Cheng, J., Jiang, B., Xie, X., Grünwald, T., Bernhofer, C. & Roupsard, O. 2017 Improving global terrestrial evapotranspiration estimation using support vector machine by integrating three process-based algorithms. *Agricultural and Forest Meteorology* **242**, 55–74.

Zhang, Z., Tian, F., Hu, H. & Yang, P. 2014 A comparison of methods for determining field evapotranspiration: photosynthesis system, sap flow, and eddy covariance. *Hydrology and Earth System Sciences* **18**, 1053–1072.

Zhao, Q., Wang, F., Zhao, J., Zhou, J., Yu, S. & Zhao, Z. 2018 Estimating forest canopy cover in black locust (*Robinia pseudoacacia* L.) plantations on the Loess Plateau using random forest. *Forests* **9**, 1–16.

http://penteli.meteo.gr/stations/amyntaio/
https://sentinel.esa.int/web/sentinel/missions/sentinel-2
fluxnet.org
https://www.sentinel-hub.com/